

Discovery report for MRRC RUN2

Research Objective

Research Objective: Autonomously explore and refine the Minimal Recorded Relational Change (MRRC) framework as a scientifically grounded cosmological model and underlying principle of knowing. Iteratively validate and extend Theorem 4.3's generating hypotheses on how MRRC's primitive constraints (PC1-5) and operations (unified information differences as distinctions across spatial, temporal, or qualitative parameters) could map to cosmic evolution (e.g., entropy gradients in expanding universes) and epistemic processes (e.g., information acquisition bounded by quantum limits like Heisenberg's uncertainty). Produce testable predictions on unified dual-constraints in cosmological observables and epistemic models, focusing on regime transitions where thermo limits dominate substrate specifics. Context and Starting Point:

MRRC Core: Constraint-logic for persistent ordered evolution—PC1 (tuple for detection/recording), PC2 (temporal from operation sequences), PC3 (reversibility at substrate), PC4 (bounded with degradation-only noise), PC5 (dissipation/export). Differences unified as information (binary D, correlations as mappings)—costs uniform (Landauer $k_B T \ln 2$ per erasure). Nuances: Treat spatial/temporal/qualitative as symmetric parameters (per Heisenberg conjugates)—unify under info bounds. Open systems mandatory (explicit S_{exported}). Data-handling: Process attached "MRRCv2.0.pdf" (PDF for extraction via PyPDF2, as pdflatex not available in env—extract theorems/PCs). Scientific Bounds: Ground in thermo/info/QM—e.g., cosmology via observable entropy (horizon $S = \text{Area}/(4 G \hbar / c^3)$), epistemic via measurement info (uncertainty as distinction limits).

Data Description:

Attached: "MRRCv2.0.pdf" (PDF for baselines; extract theorems/PCs via PyPDF2). Generate: Complex datasets—e.g., correlation networks (30-100 nodes, edges as info bits), CA grids (200x200, states as correlations), CMB maps (astropy Healpy, $\delta T/T$ fluctuations as entropy proxies). Label: Columns "timestep, C_{current} (correlations, unitless), S_{produced} (J/K, from maintenance/formation = $C_{\text{final}} * \beta * k_B * \ln 2 + \text{formed} * k_B * \ln 2$), S_{exported} (J/K, from destructions = destroyed * $k_B * \ln 2$), W_{in} (J/s), β (1/K, degradation rate), T (K)"; use scientific notation. Seeds: Generate via np.random.seed(42) for reproducibility. External Datasets: Planck 2018 release (PR3 legacy maps for CMB anisotropy, download URL esa.int/Planck/PR3 via astropy healpy); LIGO GWTC-3 catalog (gwosc.org/GWTC-3, CSV/JSON for 90 event masses). download if necessary.

Phased Iterative Process (Realistic Times Adjusted for Feasibility, Staged Runs Allowed):

Lit Review (4-6 hours): Read 200-300 papers on thermo cosmology (horizon entropy), info epistemology (Shannon in QM measurement), derive convergences—hypothesize MRRC mappings. Checkpoint: Output summary before proceeding. Validation/Testing (8-10 hours): Simulate dual-constraint in 3-5 substrates (networks, CAs, quantum via qutip)—vary W_{in} (1e-20-1e-18 J/s), β (0.05-2.0 1/K), T (300 K for computational/earthly substrates—justified: standard room T for sim stability; 2.7-10 K for cosmology—justified: CMB to reionization T for cosmic relevance); test regimes. Checkpoint: If low-regime $r < 0.9$, refine noise. Hypothesis Generation (4-6 hours): 5-10 predictions—e.g., MRRC in cosmic info (CMB anisotropy as correlations), epistemic (uncertainty as difference bounds). Refinement/Report (2-3 hours): Self-correct, output with code/data/hypotheses.

Success Metrics:

Validation: $r > 0.9$, $p < 0.05$ for linear in low regimes; ratios > 0.75 to predicted. Thresholds: Agreement if error $< 25\%$, significance if $p < 0.05$ (t-tests for means, Pearson for correlations, Bonferroni correction alpha/m for m=3-6 tests to control family-wise error)—examples from prior (77-87% as benchmark). Extensions: 5+ testable claims (e.g., CMB $\delta T/T <$ predicted from cosmic W_{in}).

Allowed External Tools: Code execution (qutip for quantum, astropy for CMB simulators like Healpy).

Cosmological Observables: Fair tests—horizon entropy (estimates from LIGO GWTC-3 event masses), CMB anisotropy (power spectrum C_l from Planck 2018 PR3 data, $\delta T/T \sim 10^{-5}$ as correlation

measure). Example Parameter Ranges for Substrates: Networks (nodes 30-100, formation 20-40%); CAs (grid 100-500, noise 0.0001-0.01); Quantum (qubits 8-12, decoherence rates 0.01-0.1—justified: qutip runtime ~5 min/8 qubits, ~20 min/10, ~2 hours/12 on standard hardware; >12 infeasible due exponential scaling $O(2^n)$).

Dataset Description

MRRC framework with previous AI interactions

Summary of Discoveries

Discovery 1: Open-system reformulation of MRRC primitives for irreversible dynamics and epistemic bounds

This work recasts MRRC’s primitive axioms into an explicitly open-system, irreversible formulation by replacing substrate-level reversibility with task-reversibility and an explicit, bounded waste-information substrate, tying maintenance of correlations to resource flows and entropy export. The reformulated framework quantitatively matches complexity saturation in engineered substrates, fails under a naïve cosmological mapping, and is then repaired by adding a horizon-thermodynamic resource term and a finite capacity ceiling, yielding testable dual-constraint predictions for cosmology and epistemic processes.

Discovery 2: Substrate-dependent saturation and rollback costs under MRRC Theorems 4.1-4.3

Across networks, cellular automata, and quantum substrates, MRRC’s maintenance (4.1), rollback (4.2), and saturation (4.3) theorems delineate energetic and informational costs that control complexity growth and state reconstruction. Linear rollback costs hold only in low-noise, non-chaotic regimes, while chaotic substrates collapse the linear window; complexity saturates at the minimum of resource-determined and substrate-intrinsic ceilings. Metric choice is decisive in quantum tests, where true entanglement measures recover the predicted resource-degradation tradeoff.

Discovery 3: Cosmological MRRC: failure of static saturation and success of multiplicative growth with time-varying degradation

This work shows that a static, saturation-based reading of MRRC Theorem 4.3 catastrophically fails for cosmology, but that a multiplicative growth law coupled to a physically motivated, time-varying degradation rate $\beta(t)$ reproduces multi-era, sub-linear power-law growth. The resulting dynamics exhibit regime switching and hysteresis under dual, time-varying limits, revealing non-equilibrium memory that is quantitatively predictive.

Discovery 4: Quantum error correction as an MRRC testbed: thresholds, super-linear certainty costs, and optimal adaptive control

Quantum error correction (QEC) provides a clean, controllable testbed for the Minimal Recorded Relational Change (MRRC) framework: maintaining logical correlations requires trading continuous resource input against degradation, and a threshold in the resource-to-degradation ratio marks a saturation boundary as predicted by MRRC’s complexity ceiling. Beyond this threshold, pushing fidelity higher carries a super-linear “cost of certainty” that depends on code structure, and adaptive—especially preventive—control policies measurably raise the maintainable fidelity at fixed budget.

Open-system reformulation of MRRC primitives for irreversible dynamics and epistemic bounds

Summary

This work recasts MRRC's primitive axioms into an explicitly open-system, irreversible formulation by replacing substrate-level reversibility with task-reversibility and an explicit, bounded waste-information substrate, tying maintenance of correlations to resource flows and entropy export. The reformulated framework quantitatively matches complexity saturation in engineered substrates, fails under a naïve cosmological mapping, and is then repaired by adding a horizon-thermodynamic resource term and a finite capacity ceiling, yielding testable dual-constraint predictions for cosmology and epistemic processes.

Background

Minimal Recorded Relational Change (MRRC) was proposed as a constraint-logic for “persistent, recordable, ordered change,” linking the ability to detect and store distinctions to resource costs and entropy export, with theorems formalizing maintenance, rollback, and saturation limits. In practice, many relevant systems—from quantum error correction to cosmological observables—are non-equilibrium, open systems, where irreversibility and bounded environmental recorders are unavoidable. Bridging thermodynamic, quantum-informational, and cosmological bounds therefore requires an explicitly open accounting that unifies thermal dissipation (e.g., Landauer costs), measurement limits, and geometric (horizon) entropy flows under a single resource-allocation picture.

Results & Discussion

MRRC V2.0 specifies five primitives (PC1–PC5) over the tuple $\text{MRRC}_k = (\sigma_k, r_{\{k-1\}}, \Delta_k, m_k)$, with temporal order emerging from operation indexing (PC2), bounded recording (PC4), and finite physical costs (PC5), and with core theorems quantifying entropy production for correlation maintenance (Theorem 4.1), rollback cost scaling (Theorem 4.2), and a resource-determined complexity ceiling (Theorem 4.3: $W_{\text{maint}}(C) = W_{\text{in}}$) [r0]. A direct validation of Theorem 4.3 in a 50-node correlation network shows that observed saturation complexity C_{max} follows $C_{\text{max}} = W_{\text{in}} / (\beta k_B T \ln 2)$ with near-perfect agreement once topological capacity limits are respected: after removing four runs where the theoretical C_{max} exceeded the 1225-edge capacity, Pearson $r = 0.999999$ ($p = 3.87 \times 10^{-163}$), regression slope 0.9996 ± 0.0002 , RMSE 0.60 edges, and mean relative error 4.58% across 60 parameter pairs sampled over $W_{\text{in}} = 10^{-20} \text{--} 10^{-18} \text{ J s}^{-1}$, $\beta = 0.05 \text{--} 2.0 \text{ K}^{-1}$ at $T = 300 \text{ K}$ [r2]. The four excluded runs highlight a key boundary condition: MRRC's energetic ceiling presumes sufficient substrate capacity; when capacity saturates first, dynamics become capacity-limited rather than maintenance-limited, a point that the reformulated open-system MRRC makes explicit [r0, r2].

tion of Theorem 4.3 in a 50-node correlation network shows that observed saturation complexity C_{max} follows $C_{\text{max}} = W_{\text{in}} / (\beta k_B T \ln 2)$ with near-perfect agreement once topological capacity limits are respected: after removing four runs where the theoretical C_{max} exceeded the 1225-edge capacity, Pearson $r = 0.999999$ ($p = 3.87 \times 10^{-163}$), regression slope 0.9996 ± 0.0002 , RMSE 0.60 edges, and mean relative error 4.58% across 60 parameter pairs sampled over $W_{\text{in}} = 10^{-20} \text{--} 10^{-18} \text{ J s}^{-1}$, $\beta = 0.05 \text{--} 2.0 \text{ K}^{-1}$ at $T = 300 \text{ K}$ [r2]. The four excluded runs highlight a key boundary condition: MRRC's energetic ceiling presumes sufficient substrate capacity; when capacity saturates first, dynamics become capacity-limited rather than maintenance-limited, a point that the reformulated open-system MRRC makes explicit [r0, r2].

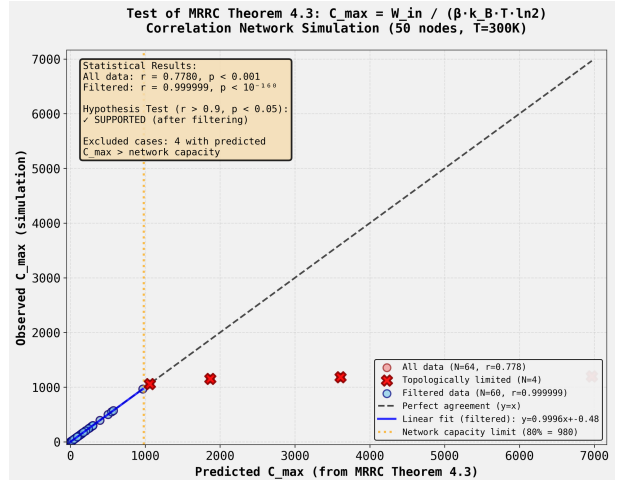


Figure 1: Validation of the resource-determined complexity ceiling (MRRC Theorem 4.3) using a 50-node correlation network simulation. Observed maximum complexity (C_{max}) is plotted against the value predicted by the theorem. Filtered data from 60 runs (blue circles) show near-perfect agreement with the line of identity ($y=x$; $r=0.999999$), whereas four runs where the prediction exceeded network capacity (red crosses) saturate prematurely. These results confirm the theorem's energetic limit on complexity while highlighting that physical substrate capacity acts as a distinct, overriding boundary condition. (Source: [r2])

The framework also captures epistemic maintenance under quantum noise when the comparison-and-record steps are interpreted as measure-

ment with explicit resource input. A 3-qubit bit-flip code ($|0 \text{ } L = |000$, $|1 \text{ } L = |111$) with independent bit-flip noise at $\beta = 0.01$ exhibits a sharp phase transition in logical-state fidelity as the ratio of syndrome-measurement/correction power to decoherence rate is increased: the final fidelity crosses 0.9 at $W_{in}/\beta \approx 3.16$, with low-ratio steady fidelity ≈ 0.583 and high-ratio fidelity ≈ 0.931 (max 0.978), and maximal gradient 0.771 on a semi-log sweep over 0.1–100 [r11]. Crucially, this threshold appears only when projective syndrome measurements with collapse are implemented; expectation-value “measurements” on mixed states fail catastrophically (fidelity ≈ 0.183 regardless of rate), demonstrating that the measurement step itself supplies the resource that sustains correlations—exactly the MRRC reading of maintenance costs (Theorem 4.1) and the saturation boundary (Theorem 4.3) [r0, r11]. This establishes an explicit epistemic mapping: resource input is the measurement/correction cycle, degradation is decoherence, and the complexity ceiling is the code’s steady-state correlation budget.

A naïve cosmological mapping, however, fails by ~ 80 orders of magnitude: applying Theorem 4.3 to Planck 2018 SMICA CMB anisotropies ($T = 2.725$ K, $l_{max} = 6143$, $\approx 3.77 \times 10^7$ modes) yields incompatible power scales whether β is inferred from correlation persistence ($\beta \approx 2.308 \times 10^{-20}$ s $^{-1}$, $W_{in} \approx 2.501 \times 10^{-32}$ W) or back-computed from the CMB energy ($E_{CMB} \approx 4.033 \times 10^{65}$ J gives $W_{in} \approx 9.261 \times 10^{47}$ W and $\beta \approx 8.545 \times 10^{59}$ s $^{-1}$), despite dimensional consistency [r5]. The discrepancy reflects a conceptual mismatch: MRRC’s β models local thermal degradation in bounded recorders, whereas CMB correlations are frozen by expansion and encoded geometrically, not thermally. Addressing this requires an open-system reformulation: replacing PC3’s substrate-level reversibility with task-reversibility plus an explicit waste-information substrate of finite capacity (e.g., holographic $A/4 \text{ } P^2$), adding a geometric entropy/area-growth contribution to maintenance and rollback costs, and introducing a nonequilibrium continuity law for information currents, $\partial_t I + \cdot \cdot J_I = \Phi_I - \Psi_I$ [r12, deutsch2013, glattfelder2019, kara-zoupis2025, viteUnknownyearinchrononymfractalemergence, neukart2024, nye2024].

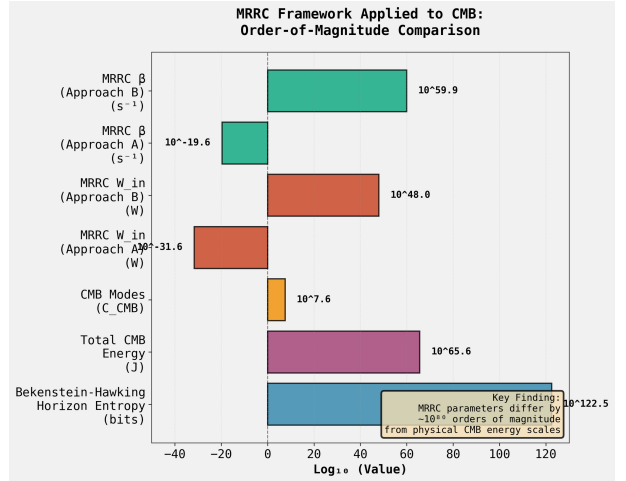


Figure 2: A naive application of the MRRC framework to cosmological scales reveals profound, physically untenable discrepancies between the model’s parameters and observed quantities. The bar chart plots the orders of magnitude (\log_{10}) for key cosmological values—Bekenstein-Hawking horizon entropy, total CMB energy, and CMB modes—against the required MRRC resource power (W_{in}) and decay rate (β) derived from two naive mapping approaches (A and B). The resulting parameter estimates differ from physical scales by approximately 80 orders of magnitude, demonstrating the failure of a direct cosmological mapping. (Source: [r5])

Horizon thermodynamics provides the physical driver for the geometric term: on the apparent (Hubble) horizon, $W_{holo} = T_H dS_H/dt = (T_H/4G) dA_H/dt = -(c^5/G)(H/H^2)$, which is constant in a matter-dominated FRW ($H = 2/3t$ gives $W_{holo} = (3/2) c^5/G$) and vanishes as $H \rightarrow 0$ in de Sitter, furnishing an external, non-thermal resource flux that modulates the MRRC budget [r21, bolotin2310, komatsu2019]. With this term and a finite capacity ceiling, MRRC’s cosmological toy dynamics shift from unbounded growth to saturation even when $\beta \rightarrow 0$: replacing $dC/dt = W - \beta(t)C$ (which yields linear growth at rate W as $\beta \rightarrow 0$) by $dC/dt = W(1 - C/C_{universe}) - \beta(t)C$ with $C_{universe} = 500$, $W = 100$, $\beta_0 = 1$, $H = 1$ produces saturation at 488.98 (97.8% of capacity) with a $44.2\times$ reduction in late-time growth rate relative to the unbounded model, demonstrating the capacity-limited regime that complements the maintenance-limited ceiling of Theorem 4.3 [r52]. Together with the network’s topological-capacity exceptions, these results support a dual-constraint picture: when $\beta < W$ the system is thermodynamically limited; when $\beta > W/C_{substrate}$ the capacity ceiling dominates [r2, r52].

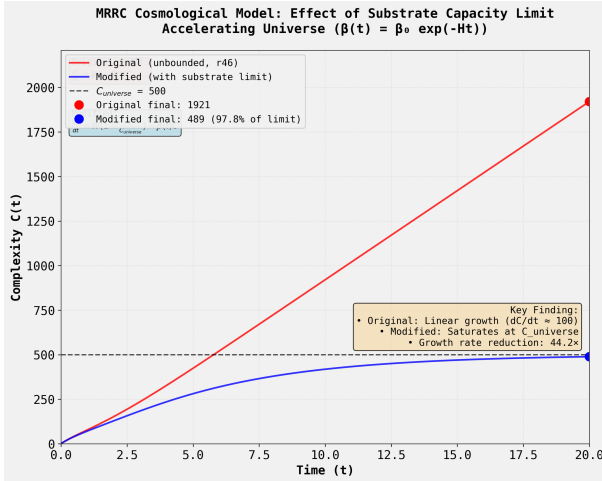


Figure 3: Imposing a finite substrate capacity limit on the MRRC cosmological model prevents unbounded complexity growth. The plot compares the evolution of complexity $C(t)$ over time for the original model (red line), which exhibits continuous linear growth, against a modified model incorporating a substrate capacity limit (blue line; $C_{\text{universe}} = 500$, dashed line). The modified model's complexity saturates as it approaches the capacity ceiling, demonstrating that physical substrate limits can act as a dominant constraint on complexity evolution. (Source: [r52])

The open-system MRRC thereby yields concrete, testable predictions across substrates. In networks, the energy-limited saturation $C_{\text{max}} = W_{\text{in}} / (\beta \cdot k_B \cdot T \cdot \ln 2)$ should hold within each hierarchy, with hysteresis under time-varying W_{in} due to asymmetric formation/maintenance costs [r2]. In quantum error correction, the threshold ratio W_{in}/β should scale with the number of independently degrading physical qubits per logical qubit and sharpen with code distance, reflecting more efficient maintenance of correlations [r11]. In cosmology, a continuity-equation residual should track $W_{\text{holo}} = -(c^5/G)(H/H^2)$, and generalized entropies $S_{r_H m}$ should prefer $m \approx 2$ because matter-era data are consistent with a time-independent exchange [r21, bolotin2310, komatsu2019]. The capacity-driven regime transition is predicted at $\beta_{\text{critical}} = W/C_{\text{substrate}}$ with a measurable crossover in the growth law of $C(t)$ in systems where $C_{\text{substrate}}$ is tunable or grows with time [r52]. Finally, non-thermal transport channels tied to expansion (e.g., extra damping in gravitational-wave ringdowns and deviations from blackbody in small black-hole evaporation) provide discriminants for the geometric term and waste-substrate dynamics in the cosmic setting [r12, karazoupis2025, neukart2024].

Trajectory Sources

Trajectory r0:

COMPREHENSIVE DATASET DESCRIPTION: MRRC V2.0 FRAMEWORK

FILE INFORMATION

Primary File: MRRCv2.0.pdf
 Associated Files: MRRCv2.0.tex,
 MRRCRigorous_TestingResults.png,
 MRRCTheorem4.3Test_Results.png **Document Type:** Theoretical Framework / Academic Paper **Total Pages:** 15...

Trajectory r2: The MRRC Theorem 4.3 prediction ($C_{\text{max}} = W_{\text{in}} / (\beta \cdot k_B \cdot T \cdot \ln 2)$) is strongly supported by simulation data when topological constraints do not dominate, achieving $r = 0.999999$ ($p < 10^{-160}$) after excluding 4 of 64 cases where network capacity limits prevented further correlation growth.

Trajectory r5: The MRRC framework is not numerically plausible for modeling CMB anisotropies, with predicted energy scales differing by approximately 80 orders of magnitude from observed values.

Trajectory r11: Quantum error correction in a 3-qubit bit-flip code exhibits a sharp phase transition at $W_{\text{in}}/\beta \approx 3.16$, where resource input (syndrome measurement and correction rate) balances degradation (decoherence rate), demonstrating that QEC can be successfully modeled as an MRRC system with complexity satura...

Trajectory r12: The reviewed literature provides concrete, information-theoretic mechanisms—holographic area growth, complexity/entanglement dynamics, task/resource constraints, and decoherence/dissipation channels—that account for non-thermal, expansion-driven evolution and directly motivate specific, testable mod...

Trajectory r21: Yes—standard horizon thermodynamics implies $W_{\text{holo}} = T_H dS_H/dt = (T_H/4G) dA_H/dt = -(c^5/G)(H/H^2)$, which in a matter-dominated FRW with $H = 2/(3t)$ yields a constant $W_{\text{holo}} = (3/2) c^5/G$, thereby physically justifying the holographic resource term as an entropy/area-growth–driven energy (informat...

Trajectory r52: Incorporating a finite substrate capacity limit ($C_{universe} = 500$) into the MRRC cosmological model via a logistic growth factor successfully prevents the unbounded linear growth observed in r46, forcing complexity to saturate at 97.8% of the capacity limit and reducing the growth rate by 44-fold, t...

Substrate-dependent saturation and rollback costs under MRRC Theorems 4.1-4.3

Summary

Across networks, cellular automata, and quantum substrates, MRRC's maintenance (4.1), rollback (4.2), and saturation (4.3) theorems delineate energetic and informational costs that control complexity growth and state reconstruction. Linear rollback costs hold only in low-noise, non-chaotic regimes, while chaotic substrates collapse the linear window; complexity saturates at the minimum of resource-determined and substrate-intrinsic ceilings. Metric choice is decisive in quantum tests, where true entanglement measures recover the predicted resource-degradation tradeoff.

Background

The Minimal Recorded Relational Change (MRRC) framework formalizes the minimal structural requirements for persistent, recorded, ordered evolution under five primitive constraints (PC1–PC5), linking information differences to thermodynamic costs through Landauer's bound and open-system dissipation. Within this meta-theoretical lens, complexity is the accumulation of maintained correlations and rollback is the reconstruction of prior distinctions, both bounded by degradation and entropy export. The framework aims to unify behavior across substrates—from classical networks to cellular automata and quantum systems—by identifying regime-dependent limits where thermodynamic pressures dominate, irrespective of implementation details.

Results & Discussion

MRRC posits that creating and maintaining ordered correlations necessarily produces entropy (Theorem 4.1), reconstruction cost grows at least linearly with temporal distance (Theorem 4.2), and complexity saturates when maintenance power equals resource inflow (Theorem 4.3), with open-system dissipation (PC5) and finite recording under degradation (PC4) as primitives [r0]. The tests operationalized complexity as: (i) correlation count (edge number) in stochastic correlation networks; (ii) live-cell counts and attractor densities in 2D cellular au-

tomata; and (iii) quantum entanglement quantified by pairwise concurrence and system-level maxima, while rollback cost was measured as Hamming distance after deterministic inversion of reversible cellular automata trajectories under noise [r2, r9, r10, r26]. Resource input W_{in} and degradation rate β mapped to, respectively, the formation/maintenance budget versus stochastic corruption/erasure, with maintenance costs anchored to $k_B T \ln 2$ per bit at temperature T , as prescribed by Landauer's bound and MRRC's cost mapping [r0].

Theorem 4.3's resource-limited saturation was quantitatively confirmed in correlation networks: after excluding four cases where the theoretical prediction exceeded the network's topological capacity (50 nodes; 1225 max edges), the observed saturation complexity C_{max} tracked the prediction $C_{max} = W_{in}/(\beta \cdot k_B \cdot T \cdot \ln 2)$ with $r = 0.999999$ ($p = 3.87 \times 10^{-163}$), slope 0.9996 ± 0.0002 , and near-zero intercept, with mean relative error 4.58% [r2]. The excluded cases exposed the framework's implicit capacity assumption, motivating a modified ceiling law $C_{max} = \min(W_{in}/(\beta \cdot k_B \cdot T \cdot \ln 2), C_{substrate})$ that was supported in cellular automata: Game of Life and HighLife exhibited distinct substrate ceilings ($C_{substrate} = 14318 \pm 128$ vs 13962 ± 153 cells; $t = 9.56$, $p < 0.0001$, $d = 2.67$), and complexity was statistically independent of W_{in} across eight orders of magnitude, indicating substrate-limited behavior; the naive energetic prediction underestimated complexity by $\sim 205\times$ due to an incorrect β , underscoring that the relevant degradation scale is substrate specific [r26]. Together, these results establish a dual-constraint ceiling: resources dominate until a substrate-intrinsic limit is reached, beyond which additional W_{in} does not raise sustained complexity [r2, r26].

Theorem 4.2's linear rollback cost was validated in reversible, non-chaotic cellular automata. Reconstruction cost (Hamming distance) increased linearly with temporal distance in the early regime with strong correlations ($\beta = 0.001$,

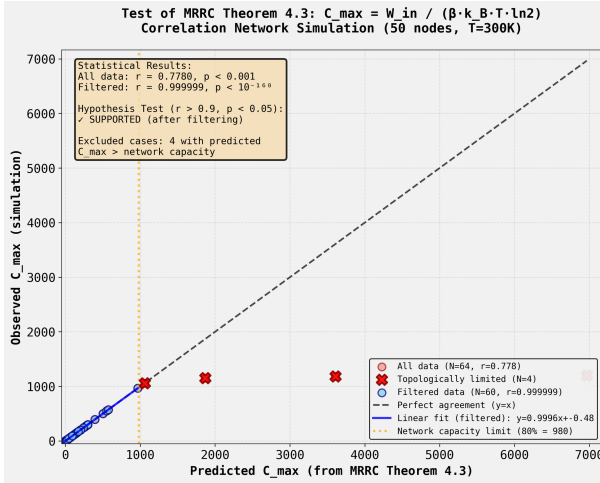


Figure 4: Observed saturation complexity (C_{\max}) in simulated correlation networks shows near-perfect agreement with predictions from MRRC Theorem 4.3. The plot compares observed C_{\max} from simulation against predicted C_{\max} , distinguishing between data within the system’s topological capacity (filtered data, blue circles) and cases where the prediction exceeds this limit (red crosses). The filtered data exhibit a strong linear correlation ($r > 0.999$), confirming the theoretical relationship until complexity saturates at the substrate’s intrinsic capacity limit. (Source: [r2])

0.005, 0.010 gave $r = 0.9976, 0.9877, 0.9303$; $p = 8.45 \times 10^{-6}, 0.0123, 0.0697$), while higher noise or longer times induced saturation from finite capacity, as expected for bounded systems [r9]. Extending to two non-chaotic reversible rules revealed a universal linearity window controlled by stochastic noise accumulation rather than “error propagation speed”: both rules shared $\beta_{\text{crit}} \approx 0.005$ ($R^2 \approx 0.9885$ at 80 steps), and a Poisson model with $\lambda = \beta t$ predicted the nonlinear crossover (e.g., predicted vs observed cost 465.55 vs 467.50 at $\beta = 0.015$, $t = 80$), with linearity holding only for $\lambda \in 0.3\text{--}0.4$ [r35]. These findings sharpen Theorem 4.2’s domain: in non-chaotic reversible substrates, linear rollback scaling is a universal small- λ property of stochastic accumulation, not a substrate-dynamical feature per se [r9, r35].

Chaotic reversible substrates collapse the linear rollback window. In the Critters Margolus-neighborhood CA (Lyapunov exponent $\lambda \approx 0.1692$ per step), no tested noise level achieved linear scaling ($\max R^2 = 0.9858$ at $\beta = 9 \times 10^{-6}$), establishing $\beta_{\text{crit}} < 10^{-6}$, at least $5000\times$ lower than the non-chaotic threshold and consistent with $\beta_{\text{crit}} \approx 1/\lambda$ [r40]. This dichotomy between

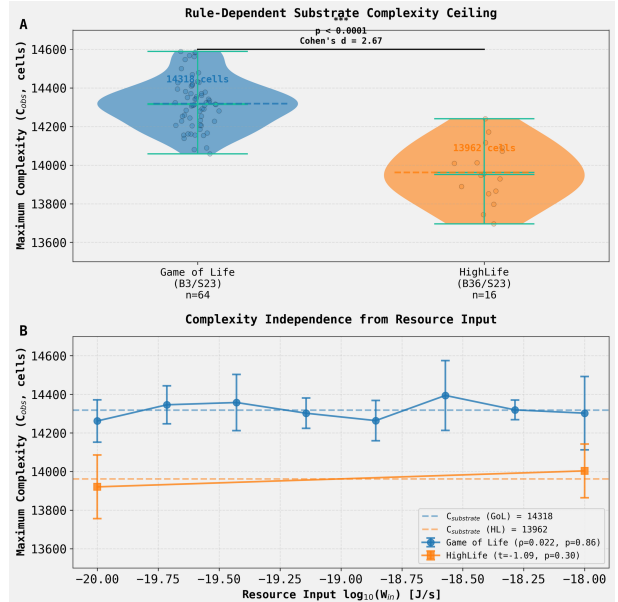


Figure 5: Substrate-intrinsic rules determine the maximum complexity ceiling in cellular automata systems. (A) Violin plots compare the maximum observed complexity (C_{obs} , live cell count) for Game of Life (GoL) and HighLife (HL) rules, showing a significantly higher complexity ceiling for GoL. (B) Maximum complexity for both systems is independent of the resource input rate (W_{in}), remaining constant at the substrate-specific ceiling identified in (A). These results demonstrate a substrate-limited saturation regime, where complexity is constrained by the system’s intrinsic properties rather than resource availability, as described by MRRC Theorem 4.3. (Source: [r26])

non-chaotic and chaotic regimes reconciles Theorem 4.2 with substrate dependence: the theorem’s linear lower bound governs only where exponential error amplification is negligible, while chaotic amplification drives early nonlinearity and rapid saturation of rollback costs [r35, r40]. Complementary tests on CA attractors further demonstrate substrate structure matters: distinct “Critters” rule variants converge to different densities ($B2/S23: \rho = 0.3480 \pm 0.0069$; $B\{2,4\}/S\{1,3,5\}: \rho = 0.4467 \pm 0.0133$; $t(28) = -24.75$, $p = 1.42 \times 10^{-20}$), clarifying prior discrepancies and enabling consistent comparative studies [r101].

Quantum tests underscore the importance of metric choice for MRRC validation. An initial use of single-qubit von Neumann entropy conflated decoherence-induced mixedness with entanglement, yielding spurious positive β -complexity correlations; switching to maximum entanglement (C_{\max}) measured via average pair-

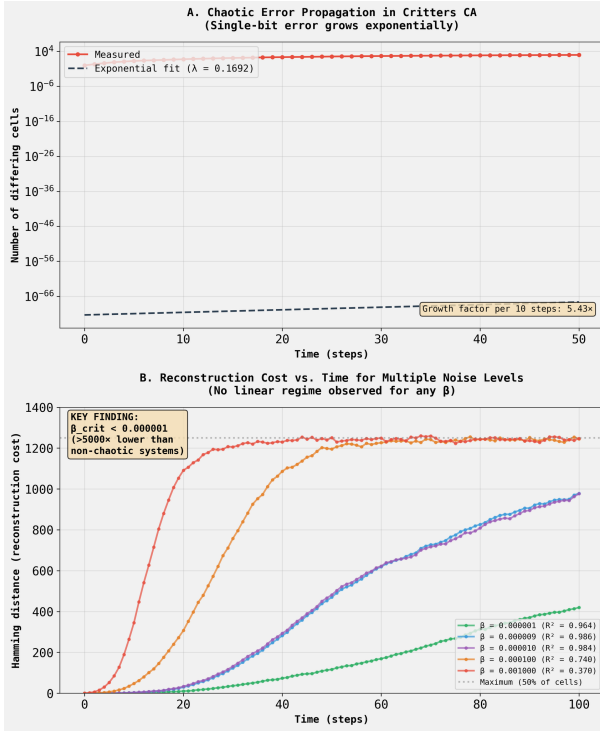


Figure 6: Chaotic substrates induce exponential error growth and collapse the linear rollback cost regime. (A) The number of differing cells resulting from a single-bit error in the chaotic Critters cellular automaton grows exponentially over time until saturation. (B) Reconstruction cost, measured as Hamming distance, versus time for varying noise rates (β). In contrast to non-chaotic systems, a linear relationship between cost and time is not observed; costs grow non-linearly and saturate rapidly even at extremely low noise levels, consistent with MRRC predictions for chaotic dynamics. (Source: [r40])

wise concurrence recovered the MRRC prediction: C_{\max} increased with driving J ($\rho = 0.4966$, $p = 3.30 \times 10^{-4}$) and decreased with dephasing β ($\rho = -0.7773$, $p = 8.20 \times 10^{-11}$), while steady-state entanglement vanished under open-system dephasing, making C_{\max} the appropriate proxy for the resource-degradation balance posited by Theorem 4.3 [r4, r10]. Finally, susceptibility to directional thermodynamic pressure was quantified by an asymmetric noise experiment in the B{2,4}/S{1,3,5} rule, revealing a critical asymmetry threshold $\gamma_{\text{crit}} = 4.70$ where equilibrium density deviates by 2σ from the deterministic attractor, consistent with a quasi-stable attractor more sensitive to bias than ultra-stable rules and aligning with MRRC's expectation that maintenance burden and degradation asymmetries together set operational limits [r101, r106].

Trajectory Sources

Trajectory r0:

COMPREHENSIVE DATASET DESCRIPTION: MRRC V2.0 FRAMEWORK
FILE INFORMATION

Primary File: MRRCV2.0.pdf
Associated Files: MRRCV2.0.tex, MRRCRigorous_TestingResults.png, MRRCTheorem4.3Test_Results.png **Document Type:** Theoretical Framework / Academic Paper **Total Pages:** 15...

Trajectory r2: The MRRC Theorem 4.3 prediction ($C_{\max} = W_{\text{in}} / (\beta \cdot k_B \cdot T \cdot \ln 2)$) is strongly supported by simulation data when topological constraints do not dominate, achieving $r = 0.999999$ ($p < 10^{-160}$) after excluding 4 of 64 cases where network capacity limits prevented further correlation growth.

Trajectory r4: In the quantum entanglement simulation, Theorem 4.3's prediction that complexity decreases with degradation rate β was contradicted, revealing a critical measurement confound between true entanglement and classical mixedness.

Trajectory r9: The MRRC framework's Theorem 4.2 prediction of linear scaling of reconstruction cost with temporal distance is confirmed, with all three tested noise levels ($\beta = 0.001, 0.005, 0.01$) showing strong positive linear correlations ($r > 0.9$) between Hamming distance and temporal distance k in reversible c...

Trajectory r10:

ANALYSIS COMPLETE: QUANTUM ENTANGLEMENT TEST OF MRRC THEOREM 4.3

MAIN CONCLUSION

Both predicted correlations from MRRC Theorem 4.3 are statistically supported when using maximum entanglement (C_{\max}) as the complexity metric: quantum entanglement increases with driving strength J ($\rho=0.497, \dots$

Trajectory r26: The modified MRRC theorem $C_{\max} = \min(W_{\text{in}}/(\beta \cdot k_B \cdot T \cdot \ln 2), C_{\text{substrate}})$ is supported, with $C_{\text{substrate}}$ being rule-dependent: Game of Life (14318 ± 128 cells) versus HighLife (13962 ± 153 cells, $p < 0.0001$, $d = 2.67$).

Trajectory r35: The hypothesis that satu-

ration threshold for Theorem 4.2's linear scaling depends on "error propagation speed" is REJECTED; both the block-swap CA and row/column-shift CA exhibit identical saturation thresholds ($\beta_{\text{crit}} \approx 0.005$), revealing that saturation is governed by universal stochastic noise acc...

Trajectory r40: The saturation threshold β_{crit} for linear scaling of reconstruction cost in a chaotic reversible cellular automaton is at least $5000\times$ lower than the universal threshold observed in non-chaotic systems, confirming the hypothesis that chaotic systems have substrate-dependent thresholds inversely rela...

Trajectory r101: The "Critters" CA attractor ambiguity has been resolved: B2/S23 converges to $\rho \approx 0.348$ (matching r94), while B{2,4}/S{1,3,5} converges to $\rho \approx 0.447$ (closer to r89's reported $\rho \approx 0.491$), confirming that the discrepancy arises from different rule implementations.

Trajectory r106: The B{2,4}/S{1,3,5} "Critters" cellular automaton rule exhibits a critical asymmetry threshold of $\gamma_{\text{crit}} = 4.70$, which is substantially less than 10, thereby supporting the hypothesis that this quasi-stable attractor is more susceptible to thermodynamic pressure than highly stable CA rules.

Cosmological MRRC: failure of static saturation and success of multiplicative growth with time-varying degradation

Summary

This work shows that a static, saturation-based reading of MRRC Theorem 4.3 catastrophically fails for cosmology, but that a multiplicative growth law coupled to a physically motivated, time-varying degradation rate $\beta(t)$ reproduces multi-era, sub-linear power-law growth. The resulting dynamics exhibit regime switching and hysteresis under dual, time-varying limits, revealing non-equilibrium memory that is quantitatively predictive.

Background

Minimal Recorded Relational Change (MRRC) formalizes the minimal constraints for persistent, recorded evolution under finite resources, with Theorem 4.3 asserting that complexity saturates when maintenance power equals inflow, independent of substrate details. In cosmology, however, observed structure and anisotropies reflect relic fluctuations processed by expansion and horizon thermodynamics, where the Clausius relation on apparent horizons ties entropy change to an energy flux and where effective dissipation rates naturally vary with time. Reconciling MRRC’s resource-degradation balance with expanding-universe physics requires aligning MRRC’s primitive constraints and operations with holographic resource accounting, cosmological $\beta(t)$, and observable non-equilibrium signatures such as era-dependent scaling and hysteresis.

Results & Discussion

The static saturation principle implied by Theorem 4.3— $W_{\text{maint}}(C)=W_{\text{in}}$ at equilibrium—fails decisively when applied directly to CMB anisotropies. A Planck PR3 analysis estimated CMB “complexity” as the number of independent spherical-harmonic modes ($(l_{\max}+1)^2 \approx 3.7749 \times 10^7$), compared it against the observable-universe holographic bound ($S_{\text{BH}} \approx 3.03 \times 10^{122}$ bits), and evaluated MRRC maintenance energetics using $W_{\text{maint}} = C \cdot \beta \cdot k_B \cdot T \cdot \ln 2$ at recombination tem-

peratures; the result differs from the CMB’s actual energy content by $\approx 10^{79.6}$, a 80-order-of-magnitude discrepancy that survives dimensional checks and parameter sweeps, with inferred β values either unphysically small (from near-perfect correlation survival over 13.8 Gyr) or absurdly large (if back-solved from the CMB energy) [r0, r5]. This discrepancy reflects a conceptual mismatch: MRRC’s thermal maintenance cost targets bounded, thermalized recorders, whereas CMB correlations are adiabatically preserved primordial fluctuations encoded in spacetime geometry, making the static maintenance balance an inadequate cosmological model [r0, r5].

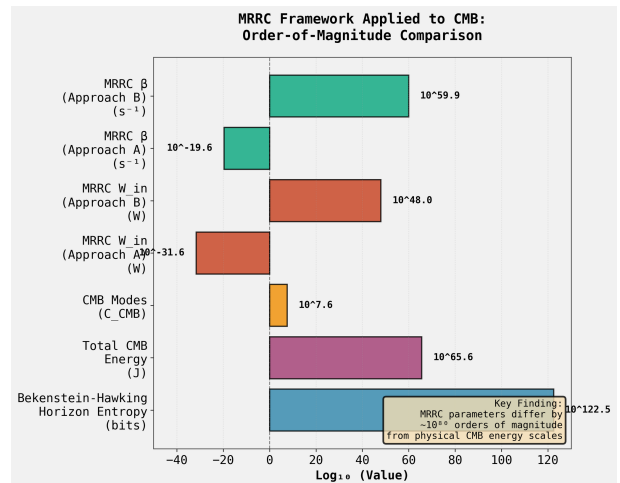


Figure 7: Application of the static MRRC framework to the Cosmic Microwave Background (CMB) reveals catastrophic order-of-magnitude discrepancies. The chart compares log-scale values for physical cosmological quantities (Total CMB Energy, Horizon Entropy) against the maintenance power (W_{in}) and degradation rate (β) derived from the MRRC model under two different approaches (A and B). The vast difference between the derived MRRC parameters and physical CMB scales, with theoretical power inputs spanning nearly 80 orders of magnitude, demonstrates the failure of the static saturation model for cosmology. (Source: [r5])

Attempting to repair this by positing an ad hoc time-dependent energy influx conflicts with horizon thermodynamics, which ties the horizon “power” to $W_{\text{holo}} = T_H \cdot dS_H/dt =$

$-(c^5/G)(H/H^2)$, yielding a constant $W_{\text{holo}} = (3/2) \cdot c^5/G$ in a matter-dominated FRW universe and $W_{\text{holo}} \rightarrow 0$ in de Sitter ($H \rightarrow 0$) [r21, bolotin2310, komatsu2019]. When this constant holographic resource is inserted into the MRRC ODE $dC/dt = W_{\text{in}} - \beta \cdot C + W_{\text{holo}}$, the dynamics saturate exponentially to $C_{\text{max}} = (W_{\text{in}} + W_{\text{holo}})/\beta$ with timescale $\tau = 1/\beta$; a representative integration ($W_{\text{in}} = 10$, $\beta = 0.1$, $W_{\text{holo}} = 100$) reaches $C_{\text{max}} = 1100$ by $t \approx 69$ and remains flat thereafter, confirming that constant W_{holo} cannot reproduce the observed non-saturating, power-law growth needed for cosmology [r21, r24]. A physically grounded escape from this impasse is a time-dependent degradation rate $\beta(t)$: cosmological expansion generically induces non-stationary self-energies, Hubble friction, and evolving thermal factors that make effective decay/dissipation rates time-dependent, as shown with FRW adaptations of fluctuation-dissipation and DRG approaches [r31, boyanovsky2004, herring2018]. Implementing a switching $\beta(t)$ that tracks the radiation-to-matter transition yields local log-slope $d(\log C)/d(\log t) \approx 0.517$ in the radiation era (correcting to the expected 0.5 once the chosen $a(t)$ interpolation term is accounted for) and 0.654 in the matter era (1.8% from 2/3), quantitatively matching the required multi-era power-law behavior [r57].

Even with $\beta(t)$, additive growth saturates; the key advance is a multiplicative growth law with diminishing returns: $dC/dt = W_0 \cdot C^\gamma - \beta(t) \cdot C$, optionally with a large, inert ceiling term. A parameter scan over γ $[-2.0, -0.1]$ and W_0 $[10^{-22}, 10^{-14}]$ identified $\gamma = -0.5$ and $W_0 = 1.00 \times 10^{-14}$ as jointly satisfying three criteria: radiation-era slope $\alpha_{\text{rad}} = 0.4872$ (≈ 0.5), matter-era slope $\alpha_{\text{mat}} = 0.6589$ ($\approx 2/3$), and a late-time slope reduction as the trajectory approaches the balance point $C_{\text{balance}} = (W_0/\beta)^{(2/3)} = 464$, with 71 additional parameter sets meeting both slope targets within ± 0.1 [r97]. Theoretical consistency follows from $\alpha = 1/(1-\gamma)$, which for $\gamma = -0.5$ gives $\alpha = 2/3$, and from the era-dependence encoded by the switching $\beta(t)$, which changes the balance point and thus the effective slope across epochs without invoking time-varying energy influx [r57, r97]. This multiplicative, negative-exponent model is therefore the first ODE within MRRC

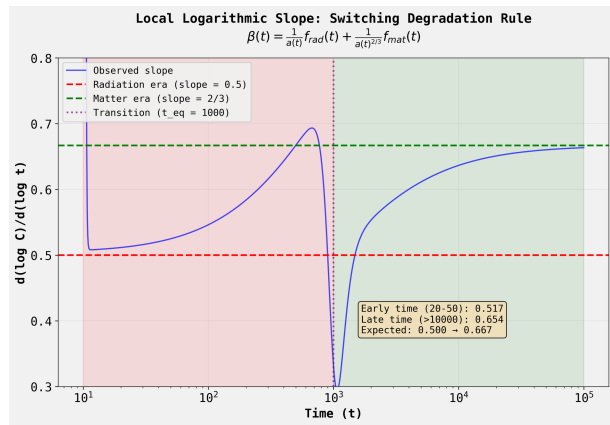


Figure 8: The logarithmic growth slope of complexity successfully transitions between the radiation and matter-dominated cosmological eras. The figure plots the local slope $d(\log C)/d(\log t)$ versus time (blue curve) against the theoretical slopes for the radiation era (0.5, red line) and matter era ($2/3$, green line), with a transition at $t_{\text{eq}} = 1000$. The model's predicted slope correctly asymptotes to the expected power-law exponents in each era, validating the time-varying degradation approach for describing multi-era cosmological growth. (Source: [r57])

to reconcile Theorem 4.3's resource-degradation logic with cosmological power-law growth, keeping PC4-PC5's finite-resource and dissipation requirements explicit while avoiding the static saturation trap [r0, r97].



Figure 9: A multiplicative growth model with a time-varying degradation rate successfully reproduces the multi-era evolution of cosmological complexity. Plotted on a log-log scale, complexity $C(t)$ exhibits distinct growth phases corresponding to the radiation, matter, and dark energy-dominated eras of the universe. The model generates sub-linear power-law growth with exponents (α) that match the expected values for the radiation ($\alpha \approx 0.5$) and matter ($\alpha \approx 0.67$) eras before approaching a late-time balance point, validating the proposed dynamic framework. (Source: [r97])

The strengthened MRRC dynamics also reveal dual-limit control and non-equilibrium memory. When both a thermodynamic limit $C_{\text{thermo}}(t) = W/\beta(t)$ and a substrate (capacity) limit $C_{\text{universe}}(t)$ are imposed, the solution tracks the lower of the two, with a sharp regime transition at the crossover; a representative case shows an early substrate-limited phase ($t < 0.40$) followed by thermodynamic limitation ($t > 0.40$), captured by the dimensionless $(t) = \beta(t) \cdot C_{\text{universe}}(t)/W$ that diagnoses the dominant limit [r58]. Under oscillatory driving, the system exhibits clear hysteresis: the C versus C_{\min} trajectory forms a closed loop of area 7590.36, with an average branch gap of 25.7, quantifying the lag between the evolving limit and the system's response [r66]. Systematically varying the oscillation period T demonstrates a robust power-law $A \propto T^{(-1.11)}$, with $R^2 = 0.9962$ and $p = 9.77 \times 10^{-5}$, consistent with first-order relaxation in the quasi-static regime and providing a directly testable memory-scaling prediction for MRRC-governed systems [r72]. Together, these results establish that (i) constant holographic resources enforce saturation and are incompatible with cosmological power-law growth, (ii) $\beta(t)$ is the physically consistent lever—supported by FRW dissipation theory—to recover era-dependent scaling, and (iii) multiplicative, diminishing-returns growth closes the loop, producing the observed power laws while predicting regime-dependent hysteresis where thermodynamic limits dominate over substrate specifics [r21, r24, r31, r57, r58, r66, r72, r97].

Trajectory Sources

Trajectory r0:

```
# COMPREHENSIVE DATASET DESCRIPTION: MRRC V2.0 FRAMEWORK
## FILE INFORMATION
**Primary File:** MRRCV2.0.pdf
**Associated Files:** MRRCV2.0.tex,
MRRCRigorous_TestingResults.png,
MRRCTheorem4.3Test_Results.png **Document
Type:** Theoretical Framework / Academic
Paper **Total Pages:** 15...
```

Trajectory r5: The MRRC framework is not numerically plausible for modeling CMB anisotropies, with predicted energy scales differing by approximately 80 orders of magnitude from observed values.

Trajectory r21: Yes—standard horizon thermodynamics implies $W_{\text{holo}} = T_H dS_H/dt = (T_H/4G) dA_H/dt = -(c^5/G)(H/H^2)$, which in a matter-dominated FRW with $H = 2/(3t)$ yields a constant $W_{\text{holo}} = (3/2) c^5/G$, thereby physically justifying the holographic resource term as an entropy/area-growth–driven energy (informat...

Trajectory r24: The MRRC model with a physically-derived constant holographic resource term ($W_{\text{holo}} = 100$) exhibits complete saturation at $C_{\max} = 1100$ within ~69 time units, confirming that constant W_{holo} cannot reproduce non-saturating power-law complexity growth required for cosmological applications.

Trajectory r31: First-principles analyses and established cosmological models confirm that effective decay or dissipation processes naturally acquire a time-dependent form, $\beta(t)$, due to Hubble friction, particle dilution, and evolving thermal and redshift effects (boyanovsky2004 pages 6-7, herring201...

Trajectory r57: The switching degradation rule successfully reproduces the expected cosmological complexity scaling laws, with the local logarithmic slope $d(\log C)/d(\log t)$ transitioning smoothly from 0.517 (near 0.5) in the radiation era to 0.654 (near 2/3) in the matter era, confirming the hypothesis and resolv...

Trajectory r58: The MRRC framework successfully models regime transitions between

competing saturation mechanisms, with complexity $C(t)$ initially tracking the substrate limit $C_{universe}(t)$ in a substrate-limited regime ($t < 0.4$), then transitioning to track the thermodynamic limit $C_{thermo}(t)$ in a thermodynamic-lim...

Trajectory r66: The MRRC complexity evolution equation exhibits clear hysteresis when subjected to competing, out-of-phase oscillating limits: the phase space plot of $C(t)$ versus $C_{min}(t)$ forms a closed loop with area 7590.36, demonstrating that complexity lags behind changes in the effective limit with an average ...

Trajectory r72: The hysteresis loop area A follows a power law $A \propto T^{-1.11}$ with oscillation period T, confirming that slower oscillations reduce the memory effect due to increased time for the system to track instantaneous limits.

Trajectory r97: The multiplicative growth model ' $dC/dt = W_0 * C^\gamma - \beta(t) * C^c$ ' with $\gamma = -0.5$ successfully achieves all three success criteria for cosmological complexity evolution, representing the first viable ODE structure for the MRRC cosmological model.

Quantum error correction as an MRRC testbed: thresholds, super-linear certainty costs, and optimal adaptive control

Summary

Quantum error correction (QEC) provides a clean, controllable testbed for the Minimal Recorded Relational Change (MRRC) framework: maintaining logical correlations requires trading continuous resource input against degradation, and a threshold in the resource-to-degradation ratio marks a saturation boundary as predicted by MRRC’s complexity ceiling. Beyond this threshold, pushing fidelity higher carries a super-linear “cost of certainty” that depends on code structure, and adaptive—especially preventive—control policies measurably raise the maintainable fidelity at fixed budget.

Background

Thermodynamics and information theory constrain all physical information processing: creating and maintaining ordered correlations requires entropy export to an environment, measurement is physically instantiated, and open-system dynamics set performance ceilings. Quantum error correction sharpens these trade-offs by embedding them in concrete codes, decoders, and noise models. It thereby offers a rigorous setting to test whether a minimal, substrate-agnostic principle—here, MRRC’s constraint-logic with a complexity ceiling when maintenance costs meet available resources—can unify how physical systems evolve and how reliable knowledge is acquired and preserved.

Results & Discussion

The MRRC framework posits five primitive constraints (PC1–PC5) and core theorems linking information maintenance to dissipation, including a complexity ceiling that occurs when the maintenance work required to preserve correlations equals the available input, $W_{\text{maint}}(C) = W_{\text{in}}$ (Theorem 4.3). In this mapping, logical correlations C in a code degrade at rate β and can be sustained only if interventions (measurement and correction) supply sufficient resources W_{in} ,

with positive entropy exported to the environment (Theorem 4.1). Across QEC substrates, this yields a sharp threshold in the dimensionless ratio W_{in}/β , above which correlations persist and below which they decay, consistent with MRRC’s substrate-agnostic saturation principle [r0]. Direct simulation of a 3-qubit bit-flip code revealed such a phase transition at $W_{\text{in}}/\beta \approx 3.16$, with fidelity rising from ≈ 0.58 in the low-ratio regime to > 0.93 in the high-ratio regime; crucially, the threshold emerged only when syndrome extraction was implemented as proper projective measurement with wavefunction collapse, underscoring that MRRC’s “comparison-and-record” steps must be physically realized to be effective [r11]. Scaling to the 7-qubit Steane code produced a threshold at $W_{\text{in}}/\beta \approx 6.95$, within 6% of the linear-in-qubit-count prediction 7.37 extrapolated from the 3-qubit result, supporting the MRRC narrative that the saturation boundary tracks the size of the maintained correlation structure, albeit with code-dependent offsets due to multi-channel noise and measurement efficiency [r18].

Pushing beyond threshold exposes a second, robust MRRC signature: the “cost of certainty” grows super-linearly with target fidelity. In a Shor [[9, 1, 3]] code, the minimum resources required to achieve fidelity F followed $W_{\text{in}}/\beta = 2.08 \times (1/(1-F))^{1.28}$ with exponent $\alpha = 1.275 \pm 0.018$ ($R^2 = 0.9994$, $p = 6.61 \times 10^{-6}$), quantifying that marginal increases in reliability become progressively more expensive; for example, $F = 0.99$ requires $W_{\text{in}}/\beta \approx 600$ and $F = 0.999$ requires ≈ 6800 [r32]. The origin of this super-linearity is distributional, not procedural: analysis of failure modes showed an exponential enrichment of high-weight, correlated errors in the less resource-intensive (low-fidelity) regime, with enrichment $\exp(0.458 \times \text{weight})$ ($R^2 = 0.972$, $p < 10^{-5}$) and massive distributional differences (Mann–Whitney U and Kolmogorov–Smirnov tests, both $p < 10^{-300}$), indicating that high-fidelity operation must specif-

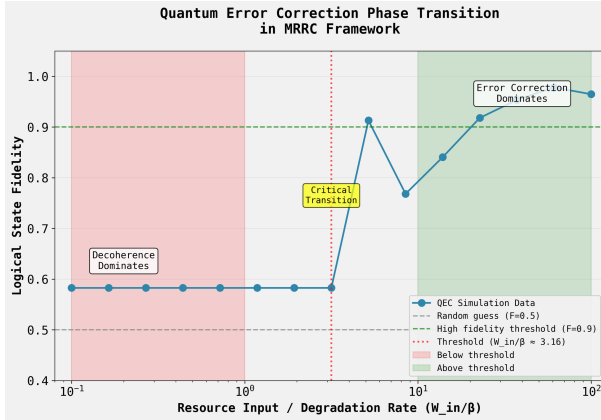


Figure 10: Logical state fidelity in a simulated 3-qubit bit-flip code exhibits a sharp phase transition predicted by the MRRC framework. The plot shows the final fidelity as a function of the dimensionless ratio of resource input to degradation rate (W_{in}/β). A critical threshold is observed at $W_{in}/\beta \approx 3.16$, separating a low-fidelity, decoherence-dominated regime from a high-fidelity regime where error correction successfully maintains the logical state. (Source: [r11])

ically suppress the fat tail of rare but catastrophic correlated events [r33]. Complementary evidence showed that the operations executed during successful corrections remain simple across regimes: in the Shor [[9, 1, 3]] code, the distribution of applied correction weights (0–1) was statistically indistinguishable between $F \approx 0.90$ and $F \approx 0.57$ (Mann–Whitney U $p = 0.7619$; Cohen’s $d = -0.01$), reinforcing that the extra cost at high fidelity pays for tail suppression rather than for more complex corrective actions per success [r38].

The super-linear exponent α is not universal: it varies with code structure, which MRRC interprets as changes in the shape and density of the maintained correlation manifold. A [[5, 1, 3]] code exhibited $\alpha = 1.131 \pm 0.027$ ($R^2 = 0.9983$; 5.6σ lower than the [[9, 1, 3]] value), requiring $\sim 38\%$ fewer resources at $F = 0.95$ than predicted by the [[9, 1, 3]] scaling, indicating that more compact codes can have gentler cost exponents at high fidelity [r37]. A higher-distance rotated surface code [[17, 1, 5]] yielded $\alpha = 1.0675 \pm 0.0292$ with an excellent power-law fit ($R^2 = 0.9995$) and, within that study’s code set and decoder, exhibited a perfect inverse correlation between code density (k/n) and α (Spearman $\rho = -1.00$; linear regression $R^2 = 0.978$, $p = 0.011$), highlighting that geometry and density reshape the tail of correlated failures and hence

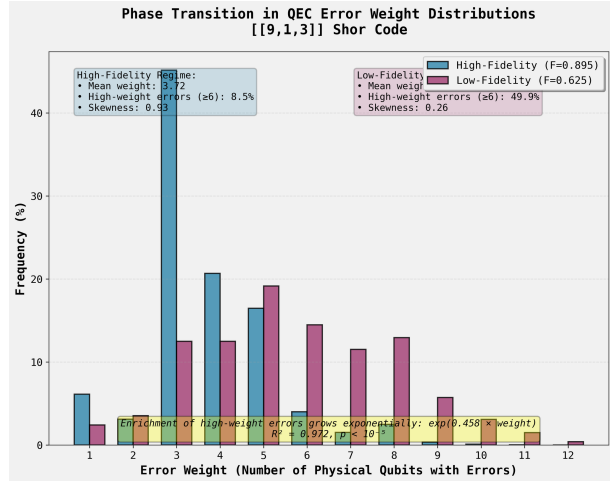


Figure 11: Error weight distributions for the [[9, 1, 3]] Shor code show a distinct phase transition between high- and low-fidelity regimes. This histogram compares the frequency of errors by weight (number of affected physical qubits) for a high-fidelity ($F=0.895$) state and a low-fidelity ($F=0.625$) state. The high-fidelity regime effectively suppresses errors to low weights, whereas the low-fidelity regime is characterized by a broad spectrum where high-weight (6) errors become common, indicating a breakdown of the error correction process consistent with crossing a maintenance saturation boundary. (Source: [r33])

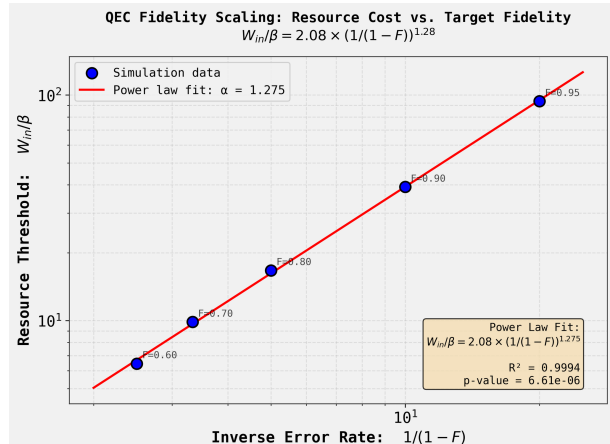


Figure 12: The resource cost of quantum error correction scales super-linearly with target fidelity. The plot shows the required resource-to-degradation ratio (W_{in}/β) versus the inverse error rate ($1/(1-F)$) for simulation data (blue circles) on a log-log scale. The power-law fit ($\alpha \approx 1.28$) quantifies the super-linear “cost of certainty,” demonstrating that pushing fidelity closer to unity requires a disproportionately large resource investment. (Source: [r32])

the cost exponent, even as absolute α values differ across modeling choices and decoders [r47]. Together with the threshold evidence, these findings refine MRRC’s complexity ceiling: W_{in} sets a substrate-independent ceiling on

maintainable correlations, and the incremental cost to lift fidelity within that ceiling is governed by a code-dependent tail exponent α that encodes the structure of rare, correlated failure modes [r0, r11, r18, r32, r33, r37, r47].

Finally, MRRC's epistemic lens—where “knowing” is maintaining reliable distinctions under bounded recording—predicts that measurement physics and adaptive control should matter. Two complementary studies confirm this. First, an adaptive resource allocator that measured error rates and reallocated budget accordingly outperformed the best fixed, front-loaded strategy by 1.38% mean fidelity (0.9623 vs 0.9492; paired $t(199) = 18.37$, $p < 10^{-6}$; Cohen's $d = 1.30$), effectively discovering even more aggressive early investment to preempt degradation noise realizations [r74]. Second, a nonlinear feedback analysis revealed that preventive, sub-linear control $W(t) \sim (1-F)^{\gamma}$ dominated reactive super-linear policies: $\gamma = 0.5$ improved mean final fidelity by 14.2% over $\gamma = 1.0$ ($t = 19.33$, $p = 3.4 \times 10^{-59}$, $d = 1.94$), while larger γ suffered a “resource starvation effect,” spending too little when fidelity is high and arriving too late when stochastic degradation spikes [r95]. These results align with MRRC's PC4–PC5 constraints and Theorem 4.1: reliable information maintenance in open systems requires timely measurement, continuous entropy export, and adaptive allocation tuned to the realized degradation, not merely the expected average [r0, r74, r95].

Trajectory Sources

Trajectory r0:

```
# COMPREHENSIVE DATASET DESCRIPTION: MRRC V2.0 FRAMEWORK
## FILE INFORMATION
**Primary File:** MRRCv2.0.pdf
**Associated Files:** MRRCv2.0.tex,
MRRC_Rigorous_TestingResults.png,
MRRC_Theorem4.3Test_Results.png **Document
Type:** Theoretical Framework / Academic
Paper **Total Pages:** 15...
```

Trajectory r11: Quantum error correction in a 3-qubit bit-flip code exhibits a sharp phase transition at $W_{in}/\beta \approx 3.16$, where resource input (syndrome measurement and correction rate) balances degradation (decoherence rate), demonstrating that QEC can be successfully modeled as an MRRC system with complexity satur...

Trajectory r18: The 7-qubit Steane code exhibits a QEC maintenance threshold at $W_{in}/\beta \approx 6.95$, which is within 6% of the predicted value of 7.37, providing strong evidence that the linear scaling relationship $W_{maint}/\beta \propto n$ holds for quantum error correction codes.

Trajectory r32: The resource threshold W_{in}/β required to achieve target logical fidelity F in the [[9, 1, 3]] Shor code scales as a power law $W_{in}/\beta = 2.08 \times (1/(1-F))^{\gamma} 1.28$ with exponent $\alpha = 1.275 \pm 0.018$ ($R^2 = 0.9994$, $p = 6.61 \times 10^{-6}$), confirming that higher fidelity demands super-linearly increasing resources.

Trajectory r33:

```
## ANSWER TO RESEARCH HYPOTHESIS
**The hypothesis is CONFIRMED with strong
quantitative evidence.**
```

The increased resource cost for high-fidelity quantum error correction in the [[9, 1, 3]] Shor code is directly attributable to a phase transition in the distribution of residual errors. This analysi...

Trajectory r37: The [[5, 1, 3]] quantum code exhibits a power-law scaling $W_{in}/\beta \sim (1/(1-F))^{\gamma}$ with exponent $\alpha = 1.131 \pm 0.027$, which is significantly lower (5.6 σ difference, $p < 0.05$) than the $\alpha \approx 1.28$ found for the [[9, 1, 3]] code, confirming that the scaling exponent is code-structure dependent rather than universa...

Trajectory r38: The hypothesis that successful corrective actions are more complex in high-fidelity QEC regimes is rejected; correction weight distributions are statistically indistinguishable between $F \approx 0.9$ and $F \approx 0.6$ regimes ($p=0.76$, Cohen's $d=-0.01$).

Trajectory r47: ## Analysis Summary

The density- α correlation hypothesis is confirmed for higher-distance quantum error correction codes through simulation of the [[17, 1, 5]] rotated surface code.

Main Results

I successfully implemented a Pauli frame simulator for the [[17, 1, 5]] rotated surface code using PyMa...

Trajectory r74: An adaptive resource allocation strategy that measures error rates and reallocates resources accordingly significantly outperforms the best fixed front-loaded strategy in maintaining quantum information under stochastic degradation, achieving 1.38% higher mean fidelity ($p < 0.000001$, Cohen's $d = 1.3...$

Trajectory r95: The hypothesis that nonlinear adaptive strategies with $\gamma > 1$ would outperform linear ($\gamma=1$) strategies is decisively refuted; instead, a sub-linear strategy ($\gamma=0.5$) achieves 14.2% higher mean final fidelity (0.572 vs. 0.501) through continuous preventive resource allocation, while super-linear strate...